# Joint PP-PS inversion at Pikes Peak oilfield, Saskatchewan

Hongbo Zhang and Gary F. Margrave

## ABSTRACT

The method of simultaneous PP-PS inversion has recently been developed and tested on the 3D Blackfoot seismic data set. This paper shows the application of this method on 3C-2D seismic data from Pikes Peak oilfield. The inversion was accomplished with a newly installed inversion module in ProMAX. After careful prestack processing, five limited-offset stacked sections for each of the vertical and radial components were created, migrated, and correlated. The inversion module assumes that the data have been trace-equalized and, to restore the average AVO behaviour, it requires the input of scalar RMS amplitude estimates for each offset. These were obtained by creating elastic synthetic seismograms for P-P and P-S from well control and calculating the RMS amplitudes for each offset. Then the ten data sets, together with the RMS amplitude values and a background velocity model, were input into the joint PP-PS AVO inversion module in ProMAX. The weighted stacking requires estimation of the P-P and P-S incidence angles at each depth level and this is done by raytracing through the background velocity model. Four attributes were determined: fractional P-wave impedance $\Delta I/I$, fractional S-wave impedance $\Delta J/J$, $\Delta(\lambda\rho)/\lambda\rho$, and $\Delta(\lambda/\mu)/(\lambda/\mu)$. Good correlation of these parameters from seismic inversion and those calculated from well logs shows that simultaneous PP-PS AVO inversion can be used to indicate anomalous lithology and pore-fluid changes in the subsurface. Therefore it should be helpful in detecting hydrocarbons using 2D multicomponent seismic data.

## INTRODUCTION

### Geology

Pikes Peak oilfield is a heavy-oil field located 40 km east of Lloydminster, Saskatchewan (Figure 1). It has been operated by Husky Energy Ltd. since 1981 and over 35 million barrels have been produced. Steam-drive technology has been used to enhance recovery. The principle of steam drive is to reduce the effective viscosity of the oil and increase the mobility in the reservoir by injecting high-temperature and -pressure steam.

Sediments of the Lower Cretaceous Mannville Gp overlie the pre-Cretaceous unconformity developed on gently southwesterly-dipping Paleozoic strata. Post-Mannville tilting to the southwest has enhanced the structural dip on the subcropping Paleozoic strata in the Lloydminster area (Orr et al., 1977). Dissolution of deep Devonian salt units around the flanks of the field set up the combination structural and stratigraphic trap. The two major producing reservoirs in the Pikes Peak field are the General Petroleum Fm and the Waseca Fm (Van Hulten, 1984). This study discusses only the Waseca oil sands that are located in the Mannville Gp and about 480 m below the surface of the Earth.
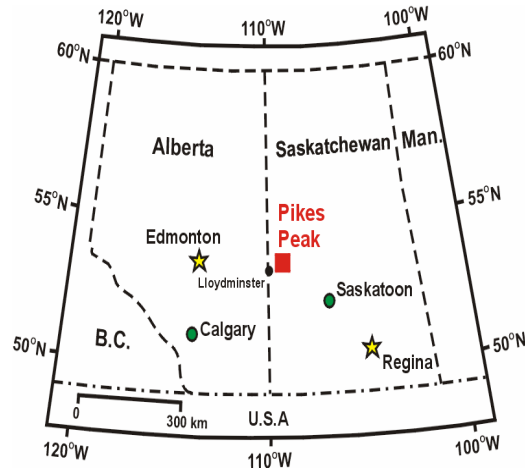
FIG. 1. Location map of the Pikes Peak oil field (edited from Hoffe et al., 2000).

The coal and sideritic shale in the McLaren and the shale at the top of the Waseca Fm form the perfect seal for the hydrocarbon in shale/sand interbed and homogeneous sand units (Van Hulten, 1984) in the middle and lower Waseca. The up-fining depositional sequences in Figure 2 demonstrate typical channel facies. The main producing zone within the Waseca Fm is the homogeneous sand unit. It ranges between 5 and 30 m of net pay within the field. The coal at the top of the Sparky Fm forms a horizon that is resistive to channel erosion. The positions of the four wells are shown in Figure 3.
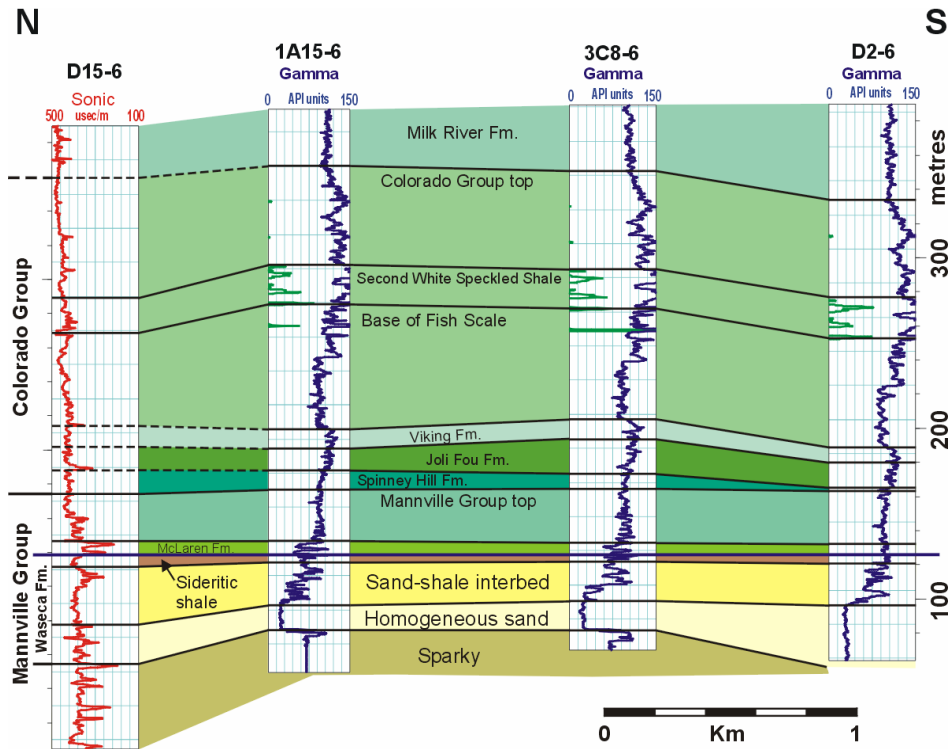


FIG. 2. Well-log cross-section illustrating the Lower Cretaceous stratigraphy (flattened at the top of the Waseca Fm). There is a channel sequence previously interpreted within the Waseca Fm (Van Hulten, 1984) and refined by the authors.

**Seismic and well-log data**

The seismic data used in this inversion project were acquired on the eastern side of the field (Figure 3) in March 2000 by the University of Calgary AOSTRA (Alberta Oil Sands Technology Research Authority) group and Husky Energy Ltd. and processed at Matrix Geoservices Ltd. For the vertical- and radial-component data used in this project, the processing-from-offset arrangement to inversion was performed by the authors and the processing before this study was carried out by Matrix Geoservices Ltd.
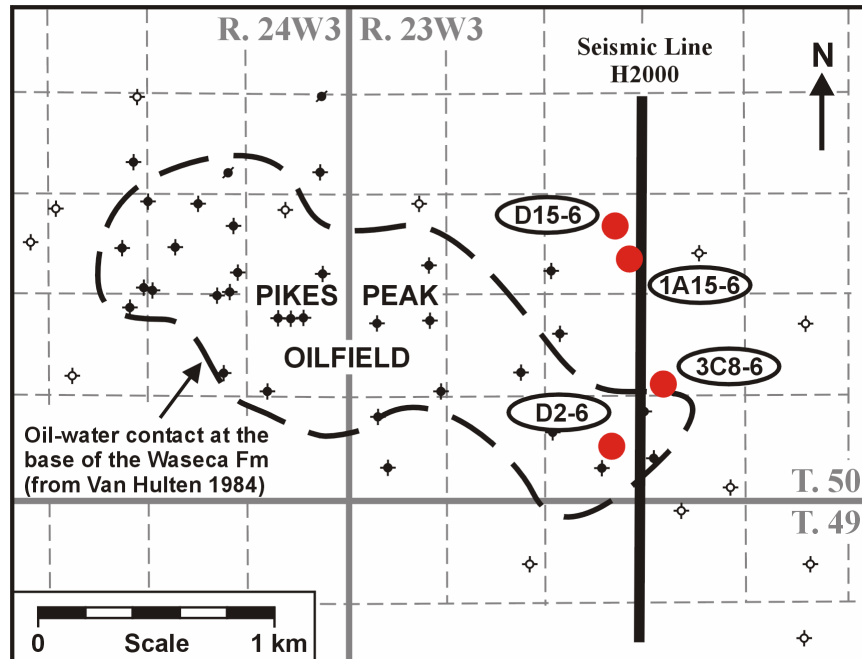


FIG. 3. Location map of the seismic line and the four wells used in this project.

While the seismic data were being acquired, pump jacks for hydrocarbon production were running constantly. The noise from pump jacks does not show up in the vertical-component data because of their high frequencies (2-150 Hz). But the noise does show up in the radial-component data due to their much lower frequencies (2-60 Hz). This is why an *f-k* filter was applied to the radial component. Careful attention was also paid to the large receiver statics present in the radial-component dataset. To solve this problem, the common-receiver stack was created so that the reflectors with small lateral changes in time were corrected. After that, residual source and receiver statics were calculated and eliminated.

The wells 1A15-6, D15-6, 3C8-6 and D2-6 were used to create synthetic P-P seismograms to tie to the P-wave seismic data due to the fact that these wells had original sonic and density logs over the Waseca interval. Well 1A15-6 was also used to tie to the converted-wave (P-S) seismic data because it had a dipole sonic log. For these data, constant-phase rotations of –45° and 90° were applied to the vertical- and radial-component data so as to give an optimal match to the synthetics.

## METHODOLOGY

The technique of joint PP-PS weighted stacking is used in the course of inversion. Stewart (1990) developed this method and Larsen et al. (1998), Larsen (1999), and Margrave et al. (2001) provided its first practical applications. The method requires migrated common-image-point gathers for both P-P and P-S reflections. These are then summed into a weighted stack, where the weights are derived from a smoothed background velocity model, to estimate fractional P and S impedance. The resulting sets of stacked sections are estimates of changes in $\Delta I/I$ and $\Delta J/J$. From these weighted stacks, such useful elastic parameters $\Delta(\lambda\rho)/\lambda\rho$ and $\Delta(\lambda/\mu)/(\lambda/\mu)$ can be derived. For the mathematical basis of this method, see Larsen (1999).

The physical basis for the method is embodied in the first-order Zoeppritz-equation approximations for plane-wave reflection and transmission coefficients. The approximations are made under the assumptions that two solid half-spaces are welded at an elastic interface, that there are only small relative changes in elastic parameters, and that the average P- and S-wave angles of incidence and transmission across the interface do not approach a critical angle or 90° (Aki and Richards, 1980). The plane-wave assumption is one that can cause inaccurate estimation of near-offset data.

The implementation of this method can be generalized as follows. First, the 3C-2D seismic data were acquired and processed to obtain high-quality, true-relative-amplitude prestack seismic data volumes. Rather than performing a full prestack migration, we NMO-corrected and stacked these into limited-offset volumes that could be poststack migrated. The more overlapping limited-offset bins are created, the higher resolution the result of the inversion will have because more detailed amplitude variation with offset will be included in the limited-offset stacked sections. But for the Pikes Peak data, if the entire offset range corresponding to the zone of interest is divided into more than five or six bins, the zone of interest cannot be completely imaged in the far-offset stacked sections. That is why we created five overlapping limited-offset bins. In order to obtain overlapping offset bins with the same interval, the number of limited-offset bins has to be odd, not even. Five of such limited-offset, migrated sections were created for both P-P and P-S reflections. For the P-P data, the absolute offset range from 0 to 759 m was divided into five overlapping bins that were 253 m wide, while for the P-S data, 284 m bins were used from 0 to 852 m.

Because true-amplitude recovery in regular processing is not perfect, trace-equalization is almost always required before stacking so the extremely strong noise does not dominate the stack. This is not a great problem for P-P AVO analysis because the average AVO behaviour is nearly constant. However, for P-S data the average AVO behaviour is roughly sinusoidal with zero at zero-offset and a maximum at some intermediate offset. Hence, it is necessary to attempt to restore the average AVO. For this purpose, P-P and P-S synthetic seismograms (Figure 4) were generated by raytracing for the traveltimes and using the Zoeppritz equations for the reflection strength.
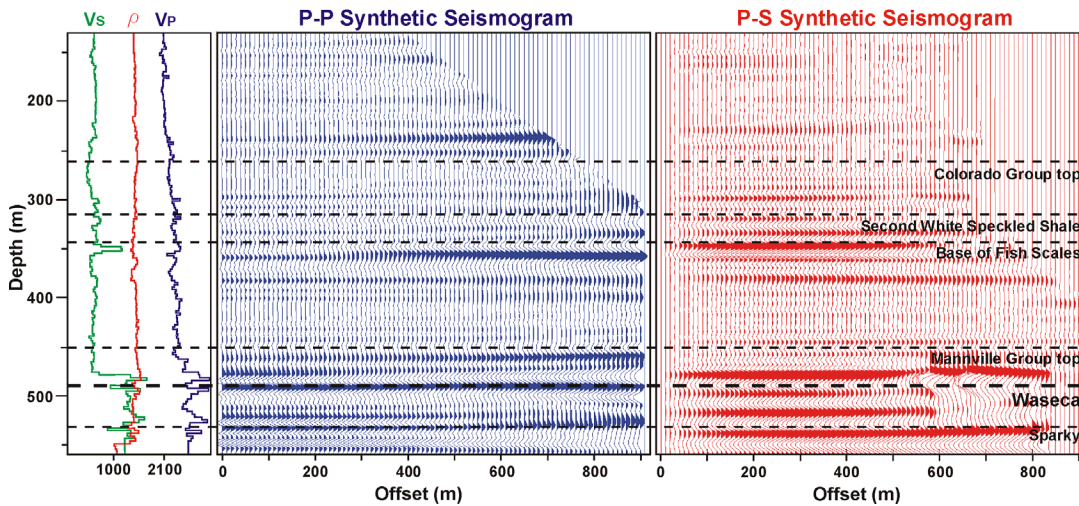
FIG. 4. Well 1A15-6 P-P and P-S synthetic seismograms used in calculating the RMS amplitude values over a range of offsets.

Then the RMS amplitude for each offset range was calculated (Figure 5) from the synthetic seismograms to obtain the average expected normalized amplitude values. Because the hydrocarbons in the zone of interest could cause dramatic changes in velocity and density, only the parts above the production zone in each sonic and density log were used in the RMS amplitude calculation. Each limited-offset migrated data volume was then rescaled to have the same RMS amplitude as the corresponding synthetic seismogram. Since migration was also applied to the stacked sections, the quality of imaging was greatly improved.
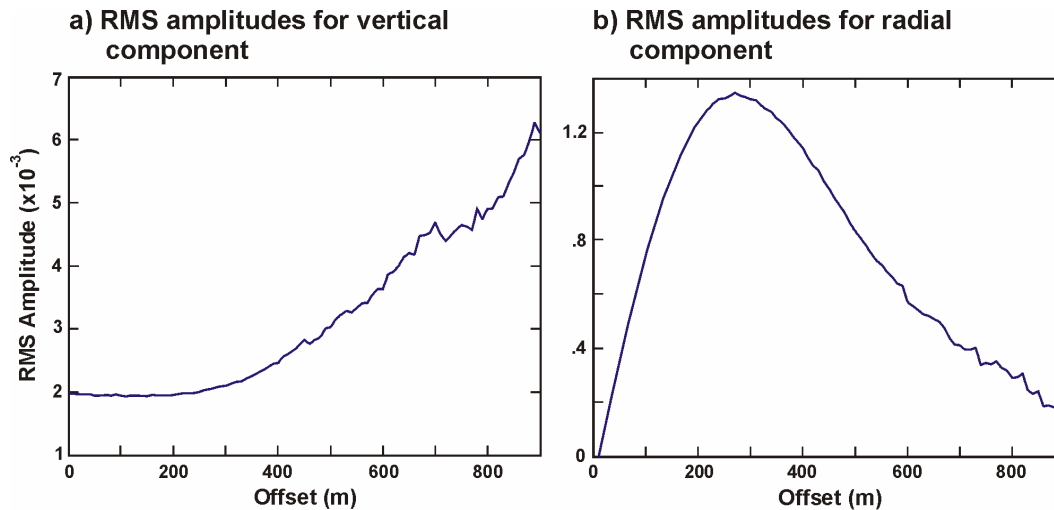


FIG. 5. RMS amplitudes versus offsets for (a) vertical and (b) radial components.

The existence of P-S seismic data highlights more information on rock properties and pore-fluid parameters in the joint inversion provided that the P-P and P-S data are very well registered. Event correlation was carried out during the course of preparing the seismic data for the joint inversion. P-P and P-S reflection events were correlated in depth by comparing them to the synthetic seismograms. But due to the frequency

difference in P-P and P-S data, the lack of very good well control and the possible complex geological structure, the event correlation may not be perfect. Hence, the ProMAX module for doing joint PP-PS AVO inversion is designed to allow the P-S seismic data to be shifted in depth relative to the P-P data so that an optimal PP-PS event correlation and thus an optimal inversion results can be achieved.

Finally, each offset data volume was weighted and they were summed together to estimate fractional P or S impedance contrasts according to the following formulae:

$$\frac{\Delta I}{I} = \sum_{offset}\left[ W_{PP\frac{\Delta I}{I}}\left(\theta_{PP},\varphi_{PP}\right)R_{PP}\left(\theta_{PP}\right) + W_{PS\frac{\Delta I}{I}}\left(\theta_{PS},\varphi_{PS}\right)R_{PS}\left(\theta_{PS}\right)\right] \qquad (1)$$

and

$$\frac{\Delta J}{J} = \sum_{offset}\left[ W_{PP\frac{\Delta J}{J}}\left(\theta_{PP},\varphi_{PP}\right)R_{PP}\left(\theta_{PP}\right) + W_{PS\frac{\Delta J}{J}}\left(\theta_{PS},\varphi_{PS}\right)R_{PS}\left(\theta_{PS}\right)\right], \qquad (2)$$

where $\theta_{PP}$ is the average of P-wave angle of incidence and reflection; $\varphi_{PP}$ is P-wave angle of transmission; $\theta_{PS}$ is the average of P-wave angle of incidence and S-wave angle of reflection; $\varphi_{PS}$ is S-wave angle of transmission. $W_{PP\frac{\Delta I}{I}}$, $W_{PS\frac{\Delta I}{I}}$, $W_{PP\frac{\Delta J}{J}}$, and $W_{PS\frac{\Delta J}{J}}$ represent the weights for P-P and P-S limited-offset stacks; $R_{PP}$ and $R_{PS}$ are respectively the observed P-P and P-S reflectivities, and $\frac{\Delta I}{I}$ and $\frac{\Delta J}{J}$ represent the fractional P-wave and S-wave impedance contrasts to be estimated. The formulae for the weights are quite complex and are not reproduced here. They may be found in Larsen (1999).

The software that carries out the simultaneous PP-PS inversion is a module called joint P-P and P-S AVO inversion in ProMAX created by X. Li in 2000 and updated and documented by D. Henley in 2002. Software packages SYNTH and LOGEDIT (CREWES proprietary software) were used to create the synthetic seismograms, Well Editor, GeoGraphix, Model Builder and CorelDraw were also used in the course of this research and the composition of this paper.

## CORRELATION OF SEISMIC INVERSION AND WELL LOG COMPUTATION

In this paper, the method of joint PP-PS AVO inversion is tested for effectiveness within the zone of interest shown in Figure 6. Correlations were conducted of the results from the simultaneous inversion and P-P standalone inversion with the attributes estimates calculated from well logs.

P-P standalone inversion is to simply examine the case of a P-P reflection and extract lithology and pore-fluid parameters from P-P seismic data only. In this case, all weights and reflectivities except weights in P-P reflectivity are set to zero. However, the P-P weights for P-P only inversion are different from the P-P weights for joint PP-PS inversion.
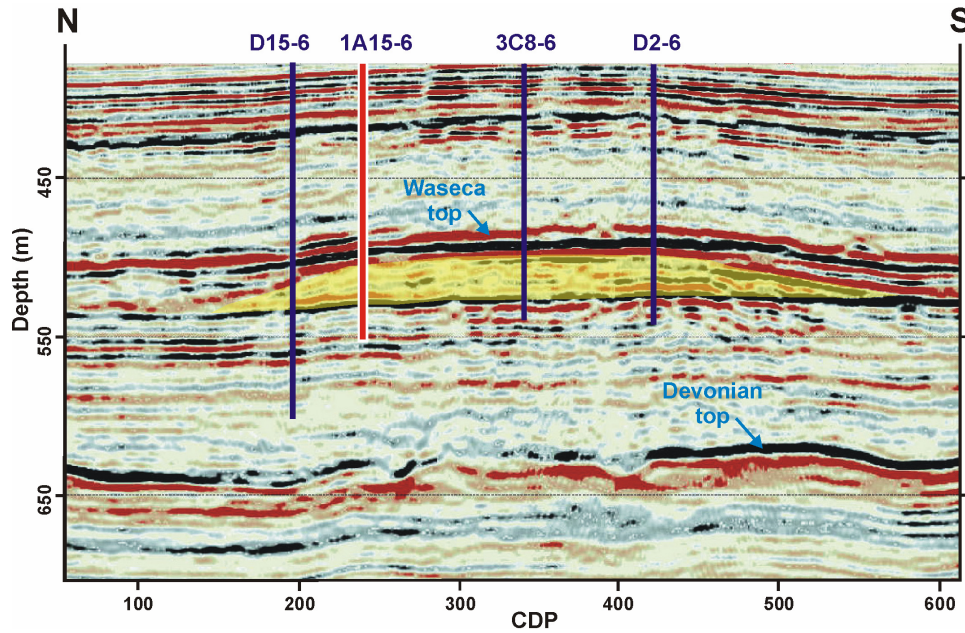
FIG. 6. The Waseca Fm reservoir (in yellow) and wells, including the dipole well 1A15-6 used in this paper.

## Fractional impedance calculation from well logs

Since the frequencies of well-log data are much higher than those of seismic data, the well logs must be smoothed and downsampled to make them directly comparable with the seismic data. First, the well-log sampling interval ($dz_2$) was increased by local averaging and decimation. The well logs were averaged over 4-m intervals for better $\Delta I/I$ and $\Delta J/J$ correlation with the results from seismic inversion. Second, the fractional impedance (P and S) contrasts are generated from these downsampled data according to equations (3) to (4) and (5) to (6) (Goodway et al., 1997), by taking ratios of the difference and average of consecutive pairs of samples:

$$\text{Fractional P-wave impedance contrast: } \frac{\Delta I}{I} = \frac{2(I_2 - I_1)}{I_2 + I_1}; \tag{3}$$

$$\text{Fractional S-wave impedance contrast: } \frac{\Delta J}{J} = \frac{2(J_2 - J_1)}{J_2 + J_1}; \tag{4}$$

$$\text{Fractional } \lambda\rho \text{ contrast: } \frac{\Delta(\lambda\rho)}{\lambda\rho} = \frac{2}{\alpha^2 - 2\beta^2}\left(\alpha^2 \frac{\Delta I}{I} - 2\beta^2 \frac{\Delta J}{J}\right); \tag{5}$$

$$\text{Fractional } \lambda/\mu \text{ contrast: } \frac{\Delta(\lambda/\mu)}{\lambda/\mu} = \frac{2\alpha^2}{\alpha^2 - 2\beta^2}\left(\frac{\Delta I}{I} - \frac{\Delta J}{J}\right); \tag{6}$$

where $\alpha$ and $\beta$ are the average P-wave and S-wave velocities across the interface, $I = \rho\alpha$, $J = \rho\beta$.

## Results of correlation

The direct well-log computations were compared to PP-PS simultaneous inversion and P-wave only inversion respectively (Figures 7-8). Generally, the correlation between simultaneous inversion and well-log computation for well 1A15-6 is fairly good around the zone of interest. In comparison, the results of P-wave only inversion are similar for $\Delta I/I$ and $\Delta(\lambda\rho)/\lambda\rho$ but quite different for $\Delta J/J$ and $\Delta(\lambda/\mu)/(\lambda/\mu)$. It seems that the joint-inversion estimates of $\Delta J/J$ and $\Delta(\lambda/\mu)/(\lambda/\mu)$ are more coherent than those from P-wave-only inversion but also of lower resolution. We do not yet know the reason for this reduced bandwidth but speculate that it is a consequence of the lower bandwidth of the P-S data. Despite this lower bandwidth, the $\Delta J/J$ and $\Delta(\lambda/\mu)/(\lambda/\mu)$ estimates from joint inversion tie to the well control better than those from P-P only.
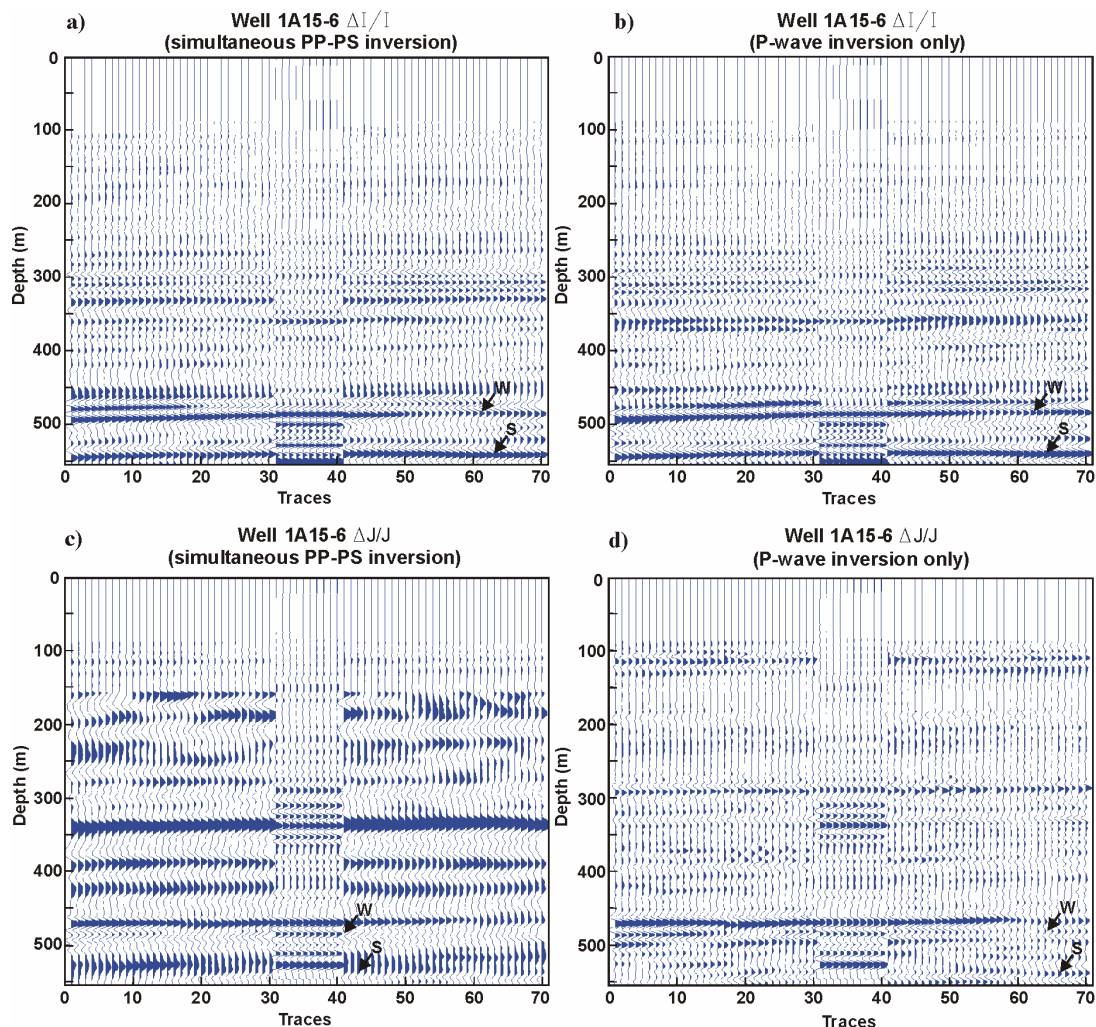


FIG. 7. Comparison of $\Delta I/I$ and $\Delta J/J$ from A15-6 well-log computation with $\Delta I/I$ and $\Delta J/J$ from a) and c), the simultaneous inversion, and b) and d), P-P standalone inversion. W-Waseca top; S-Sparky top.

Meanwhile, among the four attributes obtained by inversion, $\Delta I/I$ and $\Delta(\lambda\rho)/\lambda\rho$ are of higher frequencies and better imaging quality because they are more highly dependent upon P-P reflectivity. Conversely, $\Delta J/J$ and $\Delta(\lambda/\mu)/(\lambda/\mu)$ are of lower frequencies because they are more dependent on shear impedance contrasts.

There are some mis-ties between seismic inversion and well-log computation in either the shallow part or the part that is close to the datum. The latter may be due to phase differences between seismic and well-log computation and the steam-injection that was going on in other nearby wells. The former may be due to both lower fold for shallow seismic data and phase differences.
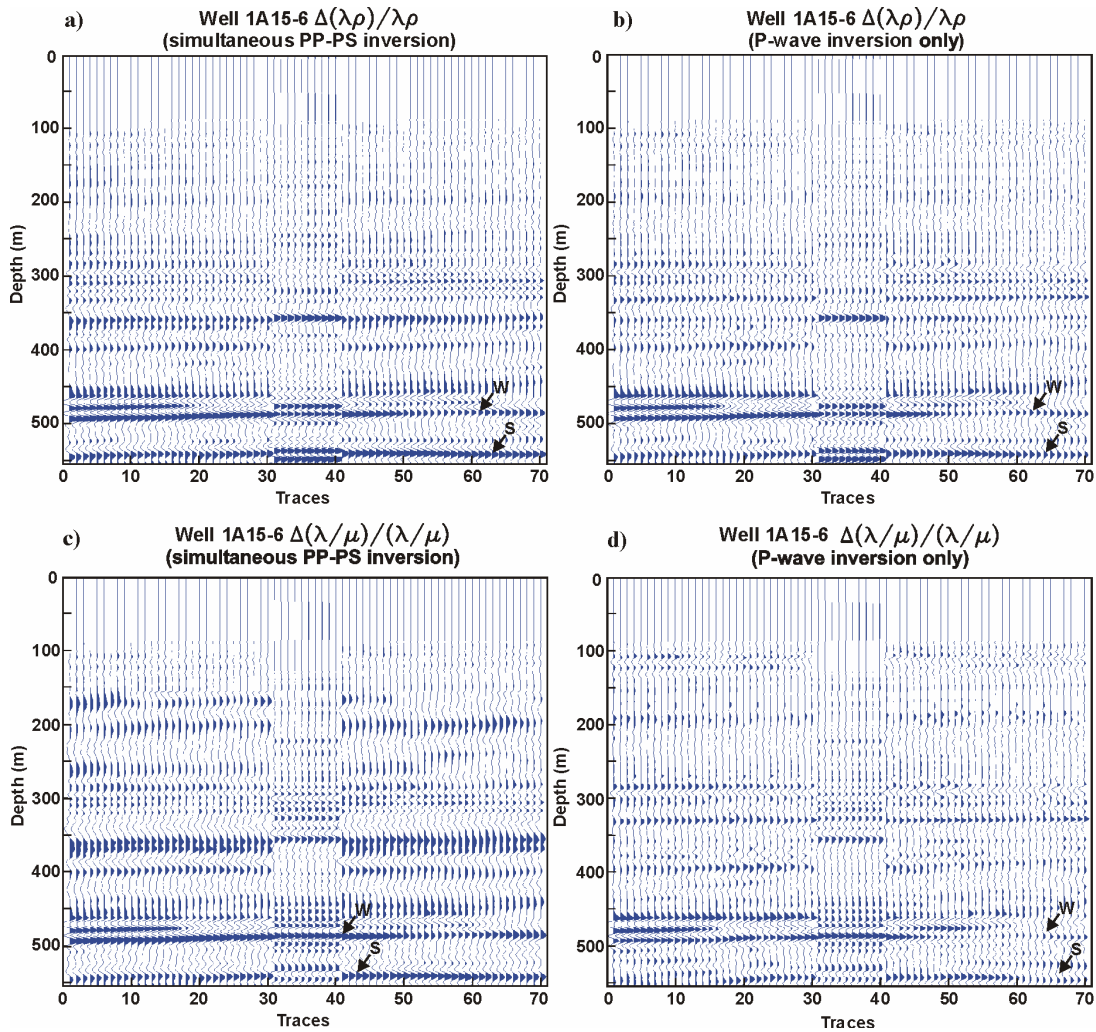


FIG. 8. Comparison of $\Delta(\lambda\rho)/\lambda\rho$ and $\Delta(\lambda/\mu)/(\lambda/\mu)$ from A15-6 well-log computation with $\Delta(\lambda\rho)/\lambda\rho$ and $\Delta(\lambda/\mu)/(\lambda/\mu)$ from a) and c), the simultaneous inversion, and b) and d), P-P standalone inversion. W-Waseca top; S-Sparky top.

## Attribute analysis

Oil was found in all four wells. Except for well D15-6, they are good producing wells. In order to find out how the inverted attributes $\Delta I/I$, $\Delta J/J$, $\Delta(\lambda\rho)/(\lambda\rho)$, and $\Delta(\lambda/\mu)/(\lambda/\mu)$ from the joint inversion respond to changes in the lithology and porefluid, the average amplitude values of the seismic traces near the four wells on the $\Delta I/I$ and $\Delta J/J$ sections were drawn into the curves after correlating the results from the simultaneous inversion with well-log computations. In cases where there is obvious channel deposition, the seismic traces within the channel were averaged. The same procedure was carried out on $\Delta(\lambda\rho)/\lambda\rho$ and $\Delta(\lambda/\mu)/(\lambda/\mu)$ sections. The changes in the average amplitude values with the changes of lithology and porefluid were investigated.

In Figure 9, we notice that when the type of lithology is mainly shale, the amplitudes of $\Delta J/J$ are greater than those of $\Delta I/I$ because of smaller elastic acoustic impedance contrast. As we approach the zone of interest, the Waseca Fm, where the sideritic shale, coal and sandstone dominate, the amplitudes of these two attributes become very close because of the more dramatic increase in the amplitude of $\Delta I/I$ than $\Delta J/J$. The shear velocity increases more dramatically than P-wave velocity at the top of the McLaren Fm, where there is a thin coal layer, and decreases in places where there is pore liquid such as oil. P-wave velocity does not decrease as much in oil but it does change more dramatically in the zone of interest where there is sand, shale, and oil. It is also possible that the much lower frequencies of the P-S reflectivity compromise the dramatic change in the shear velocity. That is why sometimes the amplitude values of $\Delta I/I$ appear to be similar or even greater than those of $\Delta J/J$. Generally, the response of $\Delta(\lambda\rho)/\lambda\rho$ and $\Delta(\lambda/\mu)/(\lambda/\mu)$ are similar to $\Delta I/I$ and $\Delta J/J$, respectively. The trend mentioned above is not exactly consistent with the direct well-log computations of these attributes. But there is an obvious increase in the amplitude of $\Delta I/I$, $\Delta J/J$ and $\Delta(\lambda/\mu)/(\lambda/\mu)$ in all four wells when the dominating lithology changes from shale to sand and coal.

In Figure 10, we zoom in on Waseca Fm on these curves. In places where the oil zones are, all the four inverted attributes appear as troughs. What is more, $\Delta I/I$ and $\Delta(\lambda/\mu)/(\lambda/\mu)$ change more dramatically than $\Delta J/J$ and $\Delta(\lambda\rho)/\lambda\rho$ when the oil zone appears in the homogeneous sand around wells 1A15-6, 3C8-6 and D2-6 that have higher producing rate. In comparison, the amplitude of $\Delta(\lambda\rho)/\lambda\rho$ is greater than $\Delta(\lambda/\mu)/(\lambda/\mu)$ when the oil zone appears in the sand-shale interbed around well D15-6.
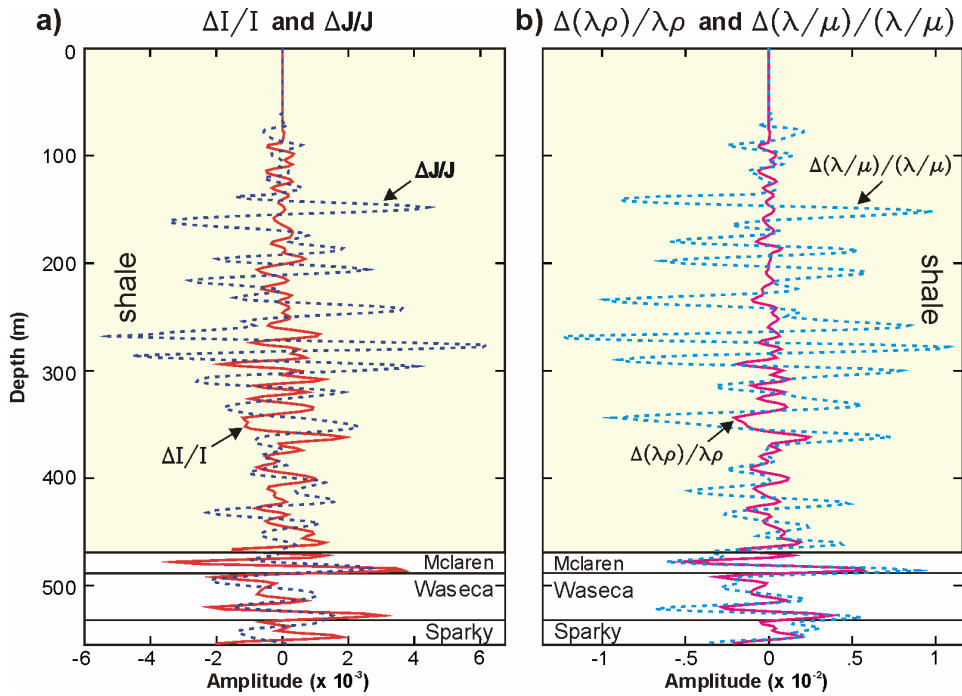
FIG. 9. Average amplitude values of a) $\Delta I/I$ and $\Delta J/J$ and b) $\Delta(\lambda\rho)/\lambda\rho$ and $\Delta(\lambda/\mu)/(\lambda/\mu)$ from traces around well 1A15-6.
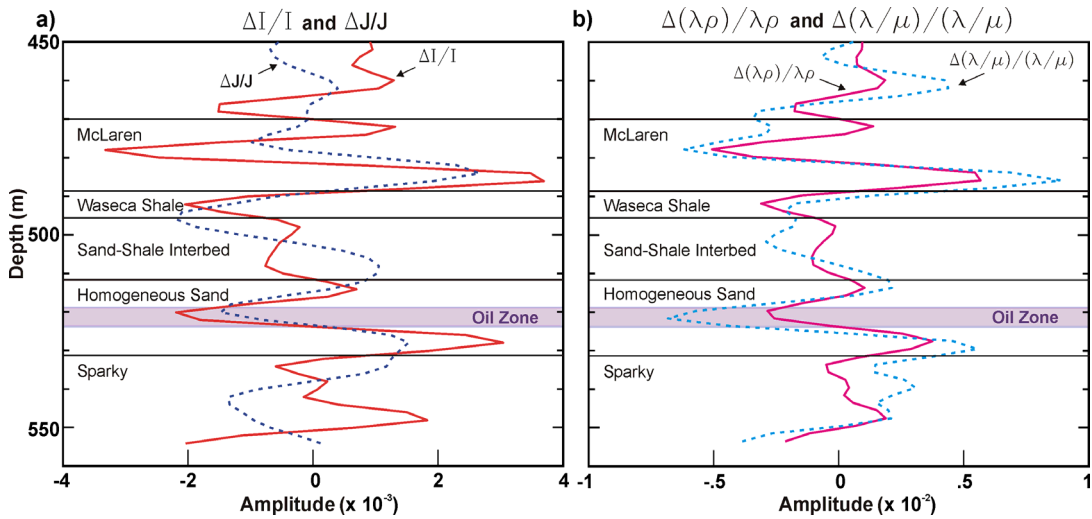


FIG. 10. Expanded attribute curves of $\Delta I/I$, $\Delta J/J$, $\Delta(\lambda\rho)/\lambda\rho$, and $\Delta(\lambda/\mu)/(\lambda/\mu)$ around well 1A15-6.

## CONCLUSIONS

A joint P-P and P-S inversion was conducted on a 2D multicomponent seismic line over the Pikes Peak oilfield. The inversion required creation of migrated, limited-offset sections for both P-P and P-S data and generation of synthetic seismograms from well control. Approximate relative amplitude restoration of the seismic data was accomplished by equalizing its RMS amplitudes with those of the synthetic seismograms for each offset. Then fractional P and S impedance contrasts were estimated by forming weighted stacks of the migrated, limited-offset sections. The success of the inversion was judged by comparing the estimated fractional impedances with direct calculations from wells.

By virtue of good correlation between simultaneous inversion and well-log computation, we conclude that the method of joint PP-PS AVO inversion worked well in this case. This could prove helpful in indicating anomalous lithology and porefluid changes in the subsurface and, thereby, in oil and gas exploration, since information contained in both P-wave and S-wave seismic data is utilized in detecting these seismic anomalies. $\Delta J/J$ and $\Delta(\lambda/\mu)/(\lambda/\mu)$ have lower resolution from joint inversion than from P-P only, but they are more coherent.

## ACKNOWLEDGEMENTS

## REFERENCES

Aki, K. and Richards, P.G., 1980, Quantitative seismology: Theory and Methods: W.H. Freeman and Company, Vol. 1.

Goodway, B., Chen, T., and Downton, J., 1997, Improved AVO fluid detection and lithology discrimination using Lame petrophysical parameters: "$\lambda\rho$", "$\mu\rho$" and "$\lambda/\mu$ fluid stack", from P and S inversions: CSEG Expanded Abstracts, 148-151.

Hoffe, B.H., Bertram, M.B., Bland, H.C., Gallant, E.V., Lines, L.R., and Mewhort, L.E., 2000, Acquisition and processing of the Pikes Peak 3C-2D seismic survey: CREWES Research Report, **12**, 511-522.

Larsen, J.A., Margrave, G.F., Lu, H., and Potter, C.C., 1998, Simultaneous P-P and P-S inversion by weighted stacking applied to the Blackfoot 3C-3D survey: CREWES Research Report, **10**, 50, 1-23.

Larsen, J.A., 1999, AVO inversion by simultaneous P-P and P-S inversion: M.Sc. Thesis, University of Calgary.

Margrave, G.F., Stewart, R.R., and Larsen, J.A., 2001, Joint PP and PS seismic inversion: The Leading Edge, **20**, 1048-1052.

Orr, R.D., Johnston, J.R., and Manko, E.M., 1977, Lower Cretaceous geology and heavy-oil potential of the Lloydminster area: Bulletin of Canadian Petroleum Geology, **25**, 1187-1221

Stewart, R.R., 1990, Joint P and P-SV inversion: CREWES Research Report, **2**, 112-115.

Van Hulten, F.F.N., 1984, Petroleum geology of Pikes Peak heavy oil field, Waseca Fm, Lower Cretaceous, Saskatchewan: Canadian Society of Petroleum Geologists, Memoir 9, 441-454.